ACS OMEGA

Open Access

http://pubs.acs.org/journal/acsodf

Article

Nanostructured ZnO with Tunable Morphology from Double-Salt Ionic Liquids as Soft Template

Md. Arif Faisal, Saika Ahmed, and Md. Abu Bin Hasan Susan*

Cite This: *ACS Omega* 2024, 9, 12992−13005

Read Online

ACCESS | Metrics & More | Article Recommendations | Supporting Information

ABSTRACT: ZnO nanostructures with tunable morphology were synthesized by the hydrothermal method from two ionic liquids (ILs), 1-ethyl-3-methylimidazolium acetate $[C_2mim]CH_3CO_2$ and 1-ethyl-3-methylimidazolium bis-(trifluoromethylsulfonyl)imide $[C_2mim](CF_3SO_2)_2N$ and their corresponding double-salt ILs (DSILs). ILs served as soft templates. DSILs were noted for the production of smaller particle size along with uniformity compared to their pure IL counterparts. A changeover of the shape of ZnO from nano-prism to a hexagonal disk-like structure was observed with the addition of $[C_2mim]CH_3CO_2$ in the medium during synthesis while nano-dice- and rod-shaped particles were obtained from $[C_2mim](CF_3SO_2)_2N$. The effect of concentration of both ILs was explored for the variations of size and shape, and at high concentrations, the morphology was distinct and sharp with uniform size in each case. The synthesized products exhibited excellent phase (wurtzite) purity and polycrystalline nature. The smallest crystallite size was acquired from DSILs, indicating the advantageous effect of the dual anions. The selective adsorption effect of $[C_2mim]CH_3CO_2$ on certain facets promoted the growth of ZnO clusters along the [1010] direction, while $[C_2mim](CF_3SO_2)_2N$ favored the growth along the [0001] direction. Consequently, DSILs rendered interpenetrating hexagonal disks due to the combined action of the anions for controlling the shape. The band gap energies of the nanoparticles (NPs) were consistent with the distribution of size. Extremely strong red emission and negligible UV emission for the synthesized ZnO NPs demonstrate their potential in the advancement of optoelectronic devices.

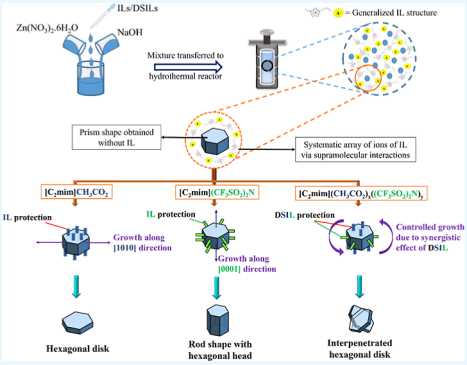

1. INTRODUCTION

Metal oxide nanoparticles (NPs), due to their unique physicochemical characteristics resulting from the quantum size effect and single electron transitions,[1−5] have emerged as the most fascinating materials in recent years. ZnO NPs have been the most successful of this type of nanostructured material with their adaptability in a range of sectors.[7,8,10,11] ZnO is a semiconductor with a broad band gap of around 3.37 eV and a significant free exciton binding energy of approximately 60 MeV.[12−14] In addition to being stable, it is environmentally beneficial. ZnO NPs have shown promise in short-wavelength optoelectronic applications, as effective adsorbents for removing a variety of toxic and hazardous chemicals and dyes,[6−8] in magnetic devices where clearly defined magnetization axes and switching fields are necessary for information storage and processing,[15,16] and in antibacterial applications.[17−19] They rank among the most promising materials for making optoelectronic devices that operate in the blue and ultraviolet (UV) regions as well as for applications involving gas sensors.[20−22] However, these structure−property relationships deeply depend on the architecture of the nanostructure of the material. Therefore, controlling the size and shape of ZnO NPs is crucial for optimizing the performance based on applications.

Synthesis of ZnO NPs with adjustable size and shape in large quantities has been a challenging task. There have been numerous attempts to create ZnO nanostructures utilizing various capping agents, such as molecular solvents, ligands, and polymers,[23−25] although the removal of such components, in particular, polymer ones from the surface of the produced ZnO NPs has been difficult. In addition, they often destroy the target NPs by rupturing the geometrical integrity of the nanostructures. Despite numerous works on the synthesis of ZnO nanoparticles using a wide range of techniques, there has truly been very few reports on the systematic control of the morphology of ZnO NPs. The proper understanding of the mechanism of formation of ZnO NPs for a controllable growth to yield targeted and desirable morphology required for versatile applications still remains a far-reaching goal.

Ionic liquids (ILs) were subsequently introduced for the production of ZnO NPs as a soft template.[26] ILs are salts

Received: November 24, 2023
Revised: December 26, 2023
Accepted: January 5, 2024
Published: March 6, 2024

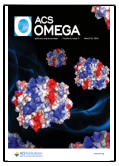

composed entirely of ions, and they remain as liquid below 100 °C or even at room temperature or far below room temperature. Good dissolving ability, low vapor pressure, good thermal stability, a highly organized liquid structure, and recyclability are the special qualities that point to the ILs acting as a soft template in the synthesis process. The most significant benefit of ILs is their ability to form highly ordered structured systems in the liquid state, which may be caused by supramolecular interactions, e.g., electrostatic attraction, $\pi-\pi$ stacking, hydrogen bonds, self-assembly, and so forth.[27−29] ILs are known as "designer solvents" since the alteration of the structure of the IL influences fascinating applications in various fields, e.g., fuel cells, dye-sensitized solar cells, electric double-layer capacitors, and lithium secondary batteries.[30,31] Similarly, by altering the structure or concentration of the IL, it is possible to create ZnO nanostructures with specific morphologies, innovative structures, and better characteristics due to the distinctive features and structures as templates or capping agents.[32−39] Furthermore, when two ILs are mixed together, the ionic associations in the individual ILs are lost, and it is difficult to distinguish ionic species or the unique interactions of the individual ILs.[40] The chemistry is solely based on the interactions between the individual ions that make up the individual ILs rather than on the identities of those ions or their interactions with the original counterions. Double-salt ILs (DSILs) are thus defined as salts containing more than one cation or anion and presenting nonideal physicochemical properties than that of the component pure ILs.[40,41] Reported studies indicate the exceptional advantages of DSIL over their component ILs in several applications.[42−50] Despite promising properties, the use of DSILs as templates for the synthesis of nanomaterials is yet to be explored. Therefore, investigation of the effects of DSIL as a template on changing the morphology of ZnO NPs could be innovative.

Herein, we aimed at exploiting the templating abilities of ILs during the synthesis of ZnO NPs and preparation of ZnO NPs with tunable size and morphology by using a simple hydrothermal method in combination with ILs of different cationic and anionic structures. A rigorous understanding of the function of ILs in regulating the shape and size of ZnO nanostructures has been developed. The introduction of DSIL as a soft template in this regard has been considered a crucial step, and the advantageous properties of DSILs have been systematically varied to provide a unique pathway for the growth of NPs and synthesize ZnO NPs with tunable morphology.

2. EXPERIMENTAL SECTION

2.1. Materials. Zinc nitrate hexahydrate ($Zn(NO_3)_2\cdot 6H_2O$) (Merck) was used as the precursor for the synthesis of ZnO NPs. Sodium hydroxide (NaOH) (Merck), 1-ethyl-3-methylimidazolium acetate $[C_2mim]CH_3CO_2$ (Sigma-Aldrich), and 1-ethyl-3-methylimidazolium bis-(trifluoromethylsulfonyl)imide $[C_2mim](CF_3SO_2)_2N$ (Sigma-Aldrich) were used as the medium for synthesis or solvent. Absolute ethanol and distilled water were used for the purpose of washing. All the chemicals were used without further purification.

2.2. Preparation of Precursors and Reagent Solutions. 1.8 M solution of $Zn(NO_3)_2\cdot 6H_2O$ and 1.8 M sodium hydroxide solution were freshly prepared by dissolving solid crystalline $Zn(NO_3)_2\cdot 6H_2O$ and NaOH pellets in water. All the aqueous solutions were prepared with deionized water (conductivity: 0.055 μS cm^{-1} at 25.0 °C) from a HPLC-grade water purification system (BOECO, Germany).

2.3. Preparation of DSILs. DSILs were prepared via straightforward mixing of the two ILs, $[C_2mim]CH_3CO_2$ and $[C_2mim](CF_3SO_2)_2N$. The DSILs were prepared at three different mole ratios. For the preparation of 5 g of $[C_2mim](CH_3CO_2)_{0.5}((CF_3SO_2)_2N)_{0.5}$, 1.5131 g of pure $[C_2mim]CH_3CO_2$ was mixed with 3.4826 g of pure $[C_2mim]$-$(CF_3SO_2)_2N$ through sonication for approximately 1.5 h. In fact, the mixture was sonicated until a single phase was obtained. Similarly, $[C_2mim](CH_3CO_2)_{0.3}((CF_3SO_2)_2N)_{0.7}$ and $[C_2mim](CH_3CO_2)_{0.7}((CF_3SO_2)_2N)_{0.3}$ were prepared by mixing appropriate amounts of pure ILs.

2.4. Synthesis of ZnO NPs from ILs and DSILs. In a typical synthesis, $Zn(NO_3)_2\cdot 6H_2O$ solution, NaOH solution, and appropriate amounts of ILs/DSILs were mixed together and stirred vigorously on a magnetic stirrer for 30 min. In the case of pure ILs, the appropriate amount added was to achieve the concentration in the range of 0.4−1.2 M in the final solution. For DSILs, the amount added was to acquire the concentration of 0.8 M. The mixture (∼35 mL) was transferred into a 75 mL Teflon container inside a stainless steel hydrothermal reactor and heated hydrothermally in an oven at 120 °C for 24 h. The hydrothermal reactor was then taken out from the oven, cooled naturally, and the resulting solid product was separated by filtration. The product was washed by absolute ethanol and distilled water several times and dried at 60 °C in air for 5 h. Finally, the solid crystalline product was stored in a vial in airtight condition.

2.5. Characterization. The synthesized products were characterized by a Fourier transform-infrared/near-infrared (FT-IR/NIR) spectrometer (Frontier, PerkinElmer) ranging from 400 to 4000 cm^{-1} by using pellets of KBr prepared with small amounts of solid materials. Elemental analysis of the products was performed via energy-dispersive X-ray spectroscopy (EDX, ZEISS Sigma 300, Germany). A computer-controlled scanning electron microscope (Hitachi S3400N) was used. A Zetasizer Nano ZS90 instrument (ZEN90, Malvern Instruments Ltd., UK) was used to analyze the size and morphology of the produced ZnO NPs. Deionized water was used as the dispersion medium for the analysis of particle size and distribution. Detailed morphological analysis was also carried out by a high-resolution transmission electron microscope (JEOL/JEM 2100) with simultaneous measurements of the selected-area electron diffraction (SAED) patterns. The phase purity and crystallinity of the ZnO NPs were evaluated using the X-ray diffraction technique. Cu Kα radiation was used to perform the diffraction measurement in order to examine the phase composition with a wide range of Bragg angles, 2θ spanning from 20 to 80°, and the model of the X-ray diffractometer used was Ultima IV. Diffuse reflectance spectroscopy (DRS) was used to record spectra using a double-beam UV−visible spectrophotometer (Model: UV-1800, Shimadzu, Japan) with an integrating sphere attachment DRA-CA-30I to determine the optical band gap energy (E_g) of the synthesized NPs. Photoluminescence spectra were recorded on a Hitachi F-7000 spectrophotometer equipped with a 150 W xenon arc lamp at room temperature. All of the samples were excited at 325 nm, and the fluorescence spectra were recorded.

https://doi.org/10.1021/acsomega.3c09374
ACS Omega 2024, 9, 12992−13005

3. RESULTS AND DISCUSSION

FTIR and EDX spectral analyses were used to show whether ZnO nanostructures were successfully prepared via hydrothermal route or not and also to indicate the possible presence of pure ILs and DSILs with the NPs due to the use of the templating strategy. The FTIR spectra of ZnO NPs are shown in Figure 1 to analyze the functional groups of the synthesized ZnO NPs prepared in different reaction media.

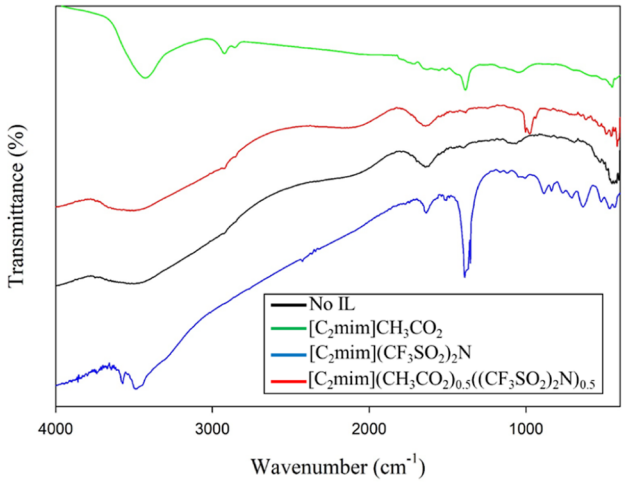

Figure 1. FTIR spectra of ZnO NPs prepared without IL; with ILs, $[C_2mim]CH_3CO_2$, and $[C_2mim](CF_3SO_2)_2N$; and with DSIL, $[C_2mim](CH_3CO_2)_{0.5}((CF_3SO_2)_2N)_{0.5}$.

The characteristic Zn−O vibration band was observed in all cases to infer the successful synthesis of ZnO NPs. Other important bands observed in the spectra, assigned in Table S1 (Supporting Information), suggest that there are ILs or DSILs present in the ZnO NPs. However, the spectra of ZnO NPs prepared with DSIL and $[C_2mim]CH_3CO_2$ are nearly free of the bands corresponding to the ILs. However, $[C_2mim](CF_3SO_2)_2N$ could not be removed completely due to its strong adsorption to the surface of the product NPs. The sharp bands of the spectrum indicate the presence of $[C_2mim](CF_3SO_2)_2N$ still being on the surface even after the application of the removal process of the ILs from the product NPs. These are also supported by the elemental analyses carried out by EDX measurements (Figure S1).

Among the ILs used in this work, $[C_2mim](CF_3SO_2)_2N$ was the most difficult one to be removed from the ZnO surface. Since the two pure ILs used in this work had the only difference in anions, the more difficulty in the removal of $[C_2mim](CF_3SO_2)_2N$ from the surface of ZnO compared to $[C_2mim]CH_3CO_2$ may be explained. The $(CF_3SO_2)_2N^-$ anion is larger in size compared to $CH_3CO_2^-$, and it has three elements (O, N, and F) in its molecular structure that can form four hydrogen bonds with the $[C_2mim]^+$ cation.[51] On the other hand, $CH_3CO_2^-$ contains only O and H to allow the formation of a smaller number of hydrogen bonds with the $[C_2mim]^+$ cation. For this reason, the $(CF_3SO_2)_2N^-$ anion tends to be accumulated more to the cation to cause enhanced adsorption on the ZnO surface. Qi et al. reported that since $Zn(NO_3)_2{\cdot}6H_2O$ and NaOH had a molar ratio of 1:1, ZnO crystals grew in a weakly acidic environment when the pH was below the isoelectric point of ZnO (IEP = 8.7−9.5).[52,53] As a result, adsorption of the $[C_2mim]^+$ cation has been considered. As a consequence, $(CF_3SO_2)_2N^-$ and $CH_3CO_2^-$ anions might adhere to the surface where they would electrostatically balance with $[C_2mim]^+$ cations. $[C_2mim](CF_3SO_2)_2N$ showed stronger adsorption on the surface of ZnO NPs, and its removal was therefore difficult from the synthesized product. Interestingly, the DSIL could be easily removed from the product NPs even though the $(CF_3SO_2)_2N^-$ anion was present in the medium. This might indicate the synergistic effect of the combined anions present in the DSIL, which enhanced the mobility of $(CF_3SO_2)_2N^-$ along with the $CH_3CO_2^-$ anion. The DSIL may thus serve as a better soft template for the synthesis of ZnO NPs and is superior to the pure ILs.

The use of different reaction media resulted in the difference in the size distribution of ZnO NPs. The analysis of size distribution was performed through DLS measurements (Figure 2). The significant variation in distribution indicates that the growth of the NPs was influenced by the presence of the IL medium.

Figure 2a,b,d shows that both the ILs follow the same trend for the change in the particle size with the increasing concentration. The smallest size was obtained at 0.8 M for both of the ILs, and a further increase in concentration resulted in a shift of the average particle size in both cases. This intermediate concentration of the pure ILs might possess a suitable environment for the production of NPs. As the nucleation of the ZnO NPs start, ILs could provide an optimum nucleation versus growth rate that the clusters of ZnO NPs might not grow further than the nanometer range. The concentration of the IL is an important parameter to tune the size of the ZnO NPs. An IL can play two roles in this process: (i) it can prevent particle agglomeration, so the reaction rate should be a little slower but still fast enough for the species to self-assemble; and (ii) it can encourage the growth of the ZnO crystal preferentially in one direction by acting as a soft template.

Since the two pure ILs have the same cationic structure and the DLS results show that the particle size followed a similar trend with the change in the concentration of the IL, the cations of the ILs are likely to serve as the controlling agents of the size. However, the effect of the anions cannot be ruled out. As seen from the DLS results, the anion $(CF_3SO_2)_2N^-$ provided a wide variation in particle size, while the size from the $CH_3CO_2^-$ anion was uniform. As discussed earlier, the $(CF_3SO_2)_2N^-$ anion is larger in size than $CH_3CO_2^-$, and these anions remain on the surface of ZnO NPs attached with the cation $[C_2mim]^+$ and get adsorbed on the ZnO surface. Thus, the anion $(CF_3SO_2)_2N^-$ could have produced a less compact arrangement and various nucleation sites for the ZnO clusters that find several ways to gather around and form particles of different sizes. On the contrary, the $CH_3CO_2^-$ anion produced a compact array and single growth direction for ZnO clusters to give rise to uniform particle size. $[C_2mim]CH_3CO_2$ thus promoted a definite direction of growth by an orderly arrangement of the ions in the reaction medium. Because of the steric hindrance caused by the larger size of the $(CF_3SO_2)_2N^-$ anion, such an orderly arrangement appears to be unlikely to cause the nucleation rate higher than the growth rate, and consequently the particle sizes were distributed in the case of $[C_2mim](CF_3SO_2)_2N$. Accordingly, $[C_2mim]CH_3CO_2$ showed better control over the nucleation rate, and hence uniform particle size along with a specific direction of growth was observed.

https://doi.org/10.1021/acsomega.3c09374
ACS Omega 2024, 9, 12992−13005

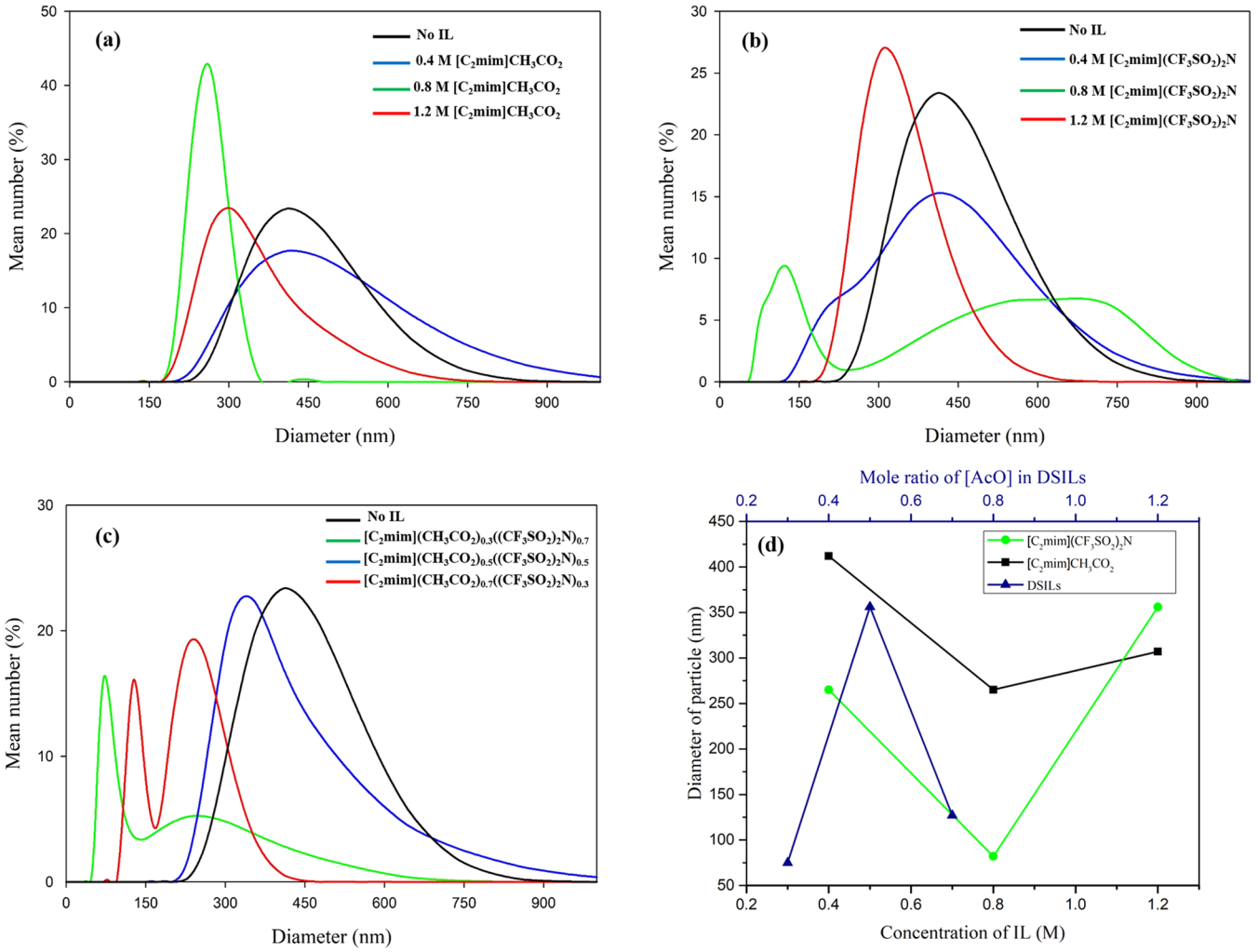

Figure 2. Particle size distribution of ZnO NPs synthesized using (a) different concentrations of $[C_2mim]CH_3CO_2$, (b) $[C_2mim](CF_3SO_2)_2N$, and (c) DSILs prepared at different mole ratios of ILs. (d) Correlation of size of the ZnO NPs with varying concentrations of pure ILs and different mole ratios of DSILs [for every concentration/mol ratio, the particles with the smallest diameter were considered].

Figure 2d shows the size distribution of ZnO NPs synthesized with DSILs. The particle size was the smallest for the DSIL, $[C_2mim](CH_3CO_2)_{0.3}((CF_3SO_2)_2N)_{0.7}$, where mole fraction is maximum for $(CF_3SO_2)_2N^-$ among all the different reaction media used in this work. In the case of $[C_2mim](CH_3CO_2)_{0.5}((CF_3SO_2)_2N)_{0.5}$, almost uniform particle size was obtained with a larger diameter of around 356 nm. Finally, for $[C_2mim](CH_3CO_2)_{0.7}((CF_3SO_2)_2N)_{0.3}$, where there is the highest mole ratio of $CH_3CO_2^-$ anion, the particle size was intermediate but without uniformity, and particles with average particle size of 127 and 229 nm could be noted. For $[C_2mim](CH_3CO_2)_{0.3}((CF_3SO_2)_2N)_{0.7}$ and $[C_2mim](CH_3CO_2)_{0.7}((CF_3SO_2)_2N)_{0.3}$, the particle size was common at 229 nm, and $[C_2mim](CH_3CO_2)_{0.3}((CF_3SO_2)_2N)_{0.7}$ yielded the smallest particles between these two DSILs. As the DSIL $[C_2mim](CH_3CO_2)_{0.3}((CF_3SO_2)_2N)_{0.7}$ gives the highest molar ratio of the $(CF_3SO_2)_2N^-$ anion, it appears that the size of most of the synthesized particles was controlled by this anion. Thus, particles of smaller size were obtained from $[C_2mim](CH_3CO_2)_{0.3}((CF_3SO_2)_2N)_{0.7}$, as supported by the observation of the smallest particle size obtained from an individual IL, $[C_2mim](CF_3SO_2)_2N$. However, when the molar ratio of the two anions was the same, i.e., for $[C_2mim](CH_3CO_2)_{0.5}((CF_3SO_2)_2N)_{0.5}$, the size was larger compared to the other two DSILs, although the particle size was uniform. The presence of $CH_3CO_2^-$ anion might diminish the tendency of the $(CF_3SO_2)_2N^-$ anion to make steric hindrance for the formation of less compacted arrangement of the ions. Thus, $[C_2mim](CH_3CO_2)_{0.5}((CF_3SO_2)_2N)_{0.5}$ provided the direction for the single growth of ZnO clusters, and the synergistic effect of the two anions is responsible for this. Clearly, the DSILs showed the effects of anions in tuning the size of the ZnO NPs.

Furthermore, for synthesizing ZnO NPs with a smaller particle size, DSILs could be the better option rather than that by using pure ILs. Evidently, the DLS results clarify that $CH_3CO_2^-$ and $(CF_3SO_2)_2N^-$ anions had their own limitations while performing separately; e.g., $CH_3CO_2^-$ anion could not produce smaller particles but provided uniform particles, while the $(CF_3SO_2)_2N^-$ anion could not provide uniformity but produced smaller particles. However, these two anions combined in DSILs performed better for the production of uniform particles with a smaller size. The self-assembly of the anions in the reaction medium for the creation of a certain growth direction was possible due to the cooperative effect of the two anions in the DSIL.

https://doi.org/10.1021/acsomega.3c09374
ACS Omega 2024, 9, 12992−13005

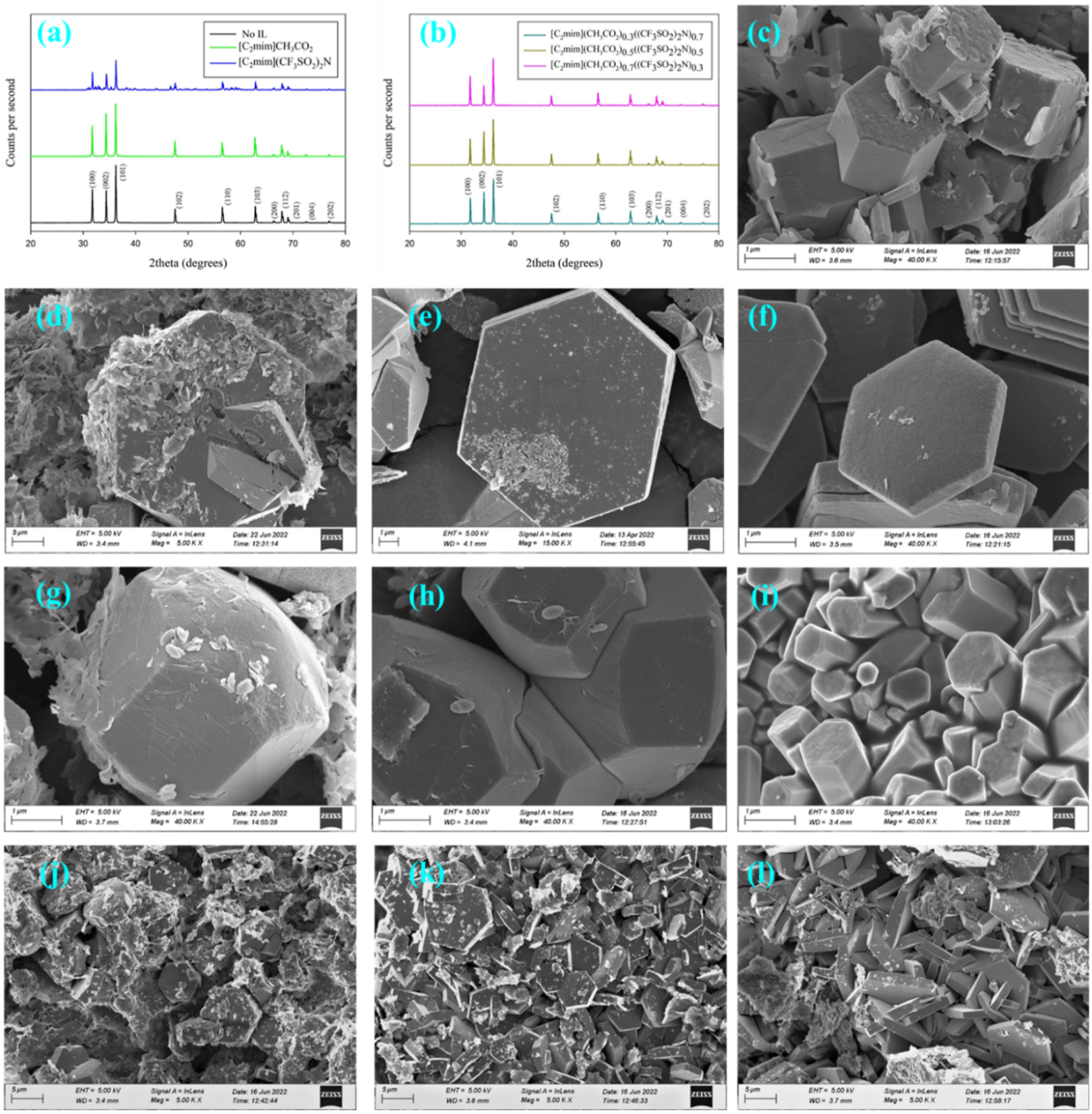

Figure 3. XRD patterns of ZnO NPs synthesized (a) without and with pure ILs and (b) with DSILs. FESEM images of ZnO NPs synthesized with (c) no IL, (d) 0.4 M $[C_2mim]CH_3CO_2$, (e) 0.8 M $[C_2mim]CH_3CO_2$, (f) 1.2 M $[C_2mim]CH_3CO_2$, (g) 0.4 M $[C_2mim](CF_3SO_2)_2N$, (h) 0.8 M $[C_2mim](CF_3SO_2)_2N$, (i) 1.2 M $[C_2mim](CF_3SO_2)_2N$, (j) $[C_2mim](CH_3CO_2)_{0.3}((CF_3SO_2)_2N)_{0.7}$, (k) $[C_2mim](CH_3CO_2)_{0.5}((CF_3SO_2)_2N)_{0.5}$, and (l) $[C_2mim](CH_3CO_2)_{0.7}((CF_3SO_2)_2N)_{0.3}$.

The crystallite size and the crystallographic phases of the ZnO NPs were determined using the XRD technique. Figure 3a,b displays the diffraction pattern of ZnO NPs after preparation using ILs and DSILs. XRD patterns suggest that the produced NPs are highly crystalline and have wurtzite structure and complete transformation of the $Zn(OH)_2$ precursor into the hexagonal wurtzite phase of ZnO. There were no sharp peaks of additional ZnO phases or contaminants. The sharp diffraction peaks illustrate the high crystallinity of the ZnO nanostructures. The NPs from the $[C_2mim](CF_3SO_2)_2N$ medium indicate the presence of little adhered impurity. Since the IL was not properly removed from the ZnO surface even after the removal treatment, it might be responsible for the residual $Zn(OH)_2$ in the sample. This is also supported by the FTIR and EDX analyses (vide infra). In general, XRD results indicate that the products are crystalline in nature with high phase purity and free of impurities such as $Zn(OH)_2$.

The crystallite size increased by the addition of pure ILs to the reaction medium (Table S2). $[C_2mim]CH_3CO_2$ provided

https://doi.org/10.1021/acsomega.3c09374
ACS Omega 2024, 9, 12992−13005

the highest crystallite size between the two pure ILs. However, the DSILs showed smaller crystallite size compared to the pure ILs as well as when there was no IL in the reaction medium. The smallest crystallite size of 69.0 nm was obtained from the DSIL, $[C_2mim](CH_3CO_2)_{0.5}((CF_3SO_2)_2N)_{0.5}$. Therefore, DSILs provided better control of NPs compared to pure ILs. Comparison of this result with the DLS measurements reveals that in some cases the hydrodynamic diameter was found to be almost the same as the crystallite size. Thus, crystallites or grains might be present in the ZnO samples which implies that in these cases the grains could not agglomerate to form particles. Specifically, in the case of 0.8 M $[C_2mim](CF_3SO_2)_2N$, the hydrodynamic diameter was found to be smaller than the crystallite size. This might have occurred due to the random growth of ZnO clusters observed in the presence of $[C_2mim](CF_3SO_2)_2N$.

To understand the growth direction of the synthesized ZnO NPs, the relative intensities of the lattice planes were analyzed. The ratios of the intensities of planes with Miller indices (002) and (100) are given in Table S3. Since the relative intensity ratios changed for different ILs and DSILs, a variation of shape can be predicted due to the certain growth direction for ZnO by each of the ILs and DSILs. As $[C_2mim]CH_3CO_2$ provided the highest ratio (1.5202), the shape could be a sort of disk like, and this changed with the variation of the IL medium. Without any IL, the ratio (0.8784) was reduced, indicating a kind of tubular shape of the particles. The DSIL, $[C_2mim](CH_3CO_2)_{0.7}((CF_3SO_2)_2N)_{0.3}$, provided the lowest value of the ratio (0.7228), suggesting the drastic change from disk-like particles. However, these results suggest that the introduction of the $CH_3CO_2^-$ anion in the reaction media caused the protection of the (001) facet and promoted the growth along the [1010] direction. This caused a sharp increase in the value of the ratio for $[C_2mim]CH_3CO_2$ compared to the case when no IL was used. On the contrary, the introduction of $(CF_3SO_2)_2N^-$ anion in the system was responsible for the protection of the lateral (100) facets to promote the growth along the [0001] direction. Nevertheless, different facets were protected by the ILs and DSILs via adsorption on the surface of ZnO NPs (vide infra). Therefore, various IL media caused different arrangements of the cations and anions promoting divergent directions for growth for the ZnO clusters.

Figure 3c–l further supports the analyses of the XRD results. Figure 3c represents the shape of small prism-like particles with hexagonal ends, as observed when no IL was used. With the addition of $[C_2mim]CH_3CO_2$, particles with hexagonal disk shape appeared as shown in Figure 3d–f. The hexagonal disks became clearer and sharper with the increase of the concentration of $[C_2mim]CH_3CO_2$. At the lowest concentration used, the hexagonal disk consisted of defects along with extremely small flakes attached on the surface. However, an increase in concentration caused less defects in the central area of the disks. Also, the edges of the hexagonal disk became sharper with the increasing concentration of the IL. A detailed geometric information on the hexagons found from $[C_2mim]CH_3CO_2$ at different concentrations is summarized in Table S4. With the increased concentration of the IL, the hexagonal disk size reduced drastically. Although perfect hexagons with the angle of almost 120° were obtained in all the concentrations, the thickness of the disks was the least at the highest concentration of the IL. In fact, all the parameters of the hexagonal disks seemed to be reduced when IL was added to the medium with increasing concentrations. Therefore, sharper hexagons were obtained for the highest concentration of the IL. This may be due to the better array construction of the cations and anions in the reaction medium which initiated the nucleation of ZnO in such a way that the growth followed the [1010] direction while increasing protection on the front and back facets of the hexagonal disk. This agrees well with the XRD results discussed above, and the presence of the $CH_3CO_2^-$ anion promoted the growth along the lateral facets. Furthermore, the increased concentration of $[C_2mim]CH_3CO_2$ might be responsible for stronger adsorption on the front and back facets of the disk which caused the growth along this direction almost diminished at higher concentrations.

For $[C_2mim](CF_3SO_2)_2N$ with varying concentrations, ZnO NPs showed variation in the shape, as shown in Figure 3g–i. The addition of 0.4 M $[C_2mim](CF_3SO_2)_2N$ to the medium provided hexagonal dice-like particles with an apex-like structure on the hexagonal front and back facets. Distorted dice-like structures were observed from 0.8 M $[C_2mim](CF_3SO_2)_2N$, which merged into one another. However, uniform shape and size were not observed in both these concentrations. At 0.4 M, capsule-like particles with diameter of 142 nm were observed. In the case of 0.8 M too, the particles were capsule-like, although the smallest diameter was 196.6 nm. This is in agreement with the results of DLS measurements. Since these shorter particles have somewhat spherical size, the nucleation rate might be greater than the growth rate as the cations and anions of $[C_2mim](CF_3SO_2)_2N$ surrounded these particles completely to separate them from other clusters to avoid growth. Although a certain growth direction was also present to provide the dice-like particles, scattered growth was observed in the case of $[C_2mim](CF_3SO_2)_2N$. However, at the highest concentration, in Figure 3i, almost smooth rodshaped particles were present with hexagonal heads. There was no other shape or size found other than nanorods in the case of the highest concentration of $[C_2mim](CF_3SO_2)_2N$. The surface of the rods was smoother than that of other particles found at a low concentration of this IL.

The presence of $CH_3CO_2^-$ anion indeed influenced the formation of disks while promoting the protection of the front and back facets by the IL. On the other hand, the $(CF_3SO_2)_2N^-$ anion initiated the formation of rodlike particles providing protection on the lateral facets. These are how the ILs provided specific growth direction while avoiding anomalous growth so that certain shape and size could be obtained. Thus, the effect of anions on the variation of shape could be understood.

The DSILs used in this work comprise one cation, $[C_2mim]^+$, and two different anions, $CH_3CO_2^-$ and $(CF_3SO_2)_2N$, at three different mole ratios. This optimization in the synthesis of ZnO NPs could be vital to understand the effect of anions on the morphological variation as well since it could be crucial to overcome the limitations observed in the pure ILs. Figure 3j–l depicts the FESEM images of ZnO nanostructures obtained from DSILs of three different compositions. For all the DSILs, the major shape of NPs was found to be hexagonal disks. However, certain parameters and arrangements of the hexagonal disks were different for various DSILs. For example, the thickness of the hexagonal disks was measured (from Figure 3j–l) and has been listed in Table S5. The thickness of the hexagonal disks gradually decreased as the content of $CH_3CO_2^-$ anion increased in the

https://doi.org/10.1021/acsomega.3c09374
ACS Omega 2024, 9, 12992−13005

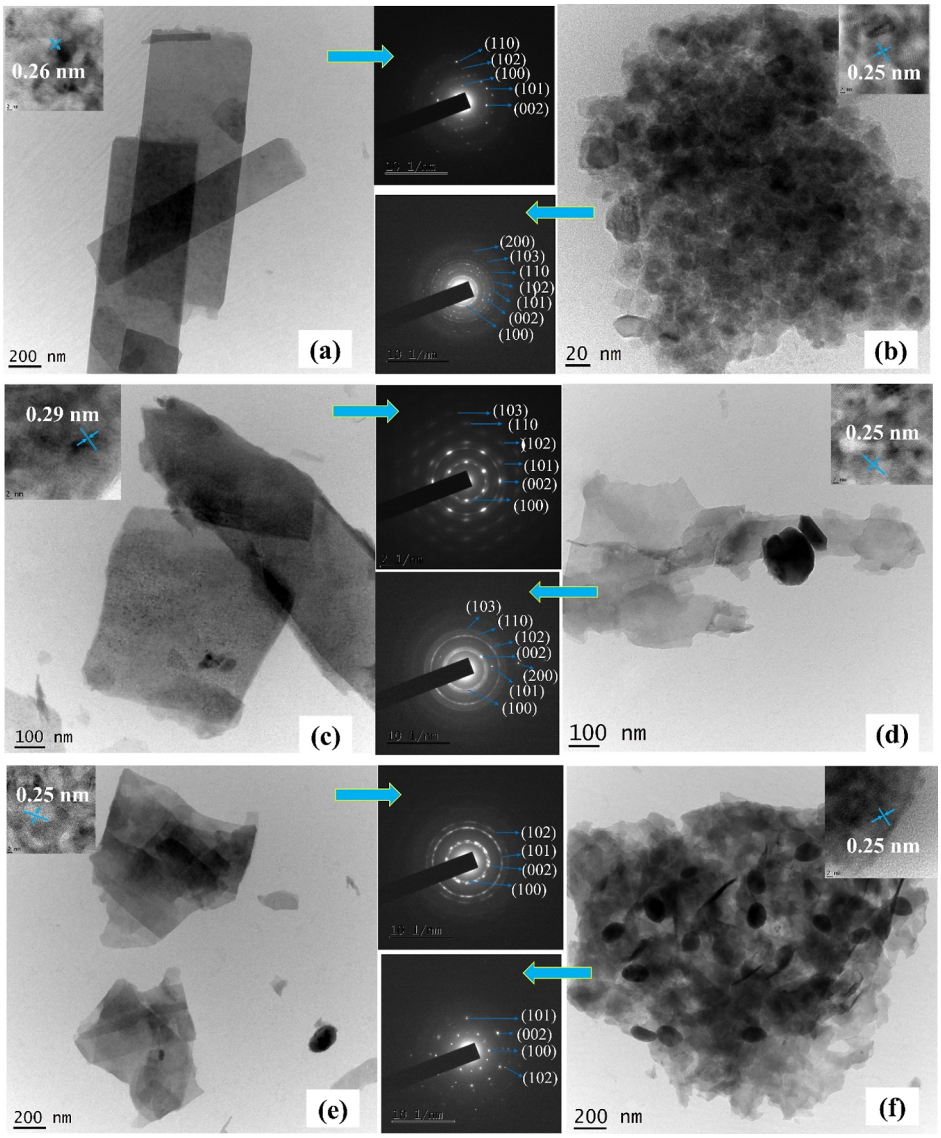

Figure 4. HRTEM images of ZnO nanostructures synthesized (a) without IL and with (b) 0.8 M $[C_2mim]CH_3CO_2$, (c) 0.8 M $[C_2mim](CF_3SO_2)_2N$, (d) $[C_2mim](CH_3CO_2)_{0.3}((CF_3SO_2)_2N)_{0.7}$, (e) $[C_2mim](CH_3CO_2)_{0.5}((CF_3SO_2)_2N)_{0.5}$, and (f) $[C_2mim]$-$(CH_3CO_2)_{0.7}((CF_3SO_2)_2N)_{0.3}$. Inset shows the SAED pattern.

DSILs. This is consistent with the result obtained from the FESEM images of the pure ILs. The tendency of the $CH_3CO_2^-$ anion was to form thinner disks as it tended to avoid growth on the front and back facets of the disks. On the contrary, the $(CF_3SO_2)_2N^-$ anion provided dice- or rod-shaped particles with hexagonal heads which are nothing but hexagonal disks with increased thickness. The presence of hexagonal disks in each of the FESEM images suggests that the $CH_3CO_2^-$ anion might act dominantly over $(CF_3SO_2)_2N^-$, since basically all the DSILs produced hexagonal disks with slight variations. For $[C_2mim](CH_3CO_2)_{0.3}((CF_3SO_2)_2N)_{0.7}$, hexagonal disks were found to be separated from one another, but in the cases of $[C_2mim](CH_3CO_2)_{0.5}((CF_3SO_2)_2N)_{0.5}$ and $[C_2mim]$-$(CH_3CO_2)_{0.7}((CF_3SO_2)_2N)_{0.3}$, the disks became interpenetrated among themselves. For $[C_2mim]$-$(CH_3CO_2)_{0.5}((CF_3SO_2)_2N)_{0.5}$, this interpenetration was initiated, and it got pretty continuous when $[C_2mim](CH_3CO_2)_{0.7}((CF_3SO_2)_2N)_{0.3}$ was used. It seems that as the $CH_3CO_2^-$ anion content was increasing in the DSILs, the hexagonal disks were coming closer and closer, and then they penetrated into each other. The penetration occurred as seen in Figure S2, where there is a specific hole that corresponds to the penetration caused by the disk above it. Also, interpenetrated disks are seen in Figure 3l. Thus, when the $CH_3CO_2^-$ anion content was growing in the DSILs, the hexagonal disks became thinner and interpenetrated into each other. Pure $[C_2mim]CH_3CO_2$, on the other hand, preferably produced disks with distance from one another. However, in the case of DSILs, the disks seemed to come closer and eventually got into each other. Probably, the reason behind this is the presence of $(CF_3SO_2)_2N^-$ anion. The dices or rodlike particles obtained from pure $[C_2mim](CF_3SO_2)_2N$ were found to gather or merge with one another. An identical behavior is seen in the cases of DSILs. However, this is observable mostly in the case of $[C_2mim](CH_3CO_2)_{0.7}((CF_3SO_2)_2N)_{0.3}$, where the amount of $(CF_3SO_2)_2N^-$ anion present is the least. Therefore, the combined effect of these two anions preferred the penetration of the hexagonal disks rather than only one anion influencing this behavior. The combined protection of the two anions might also cover almost the whole lateral facets

https://doi.org/10.1021/acsomega.3c09374
ACS Omega 2024, 9, 12992−13005

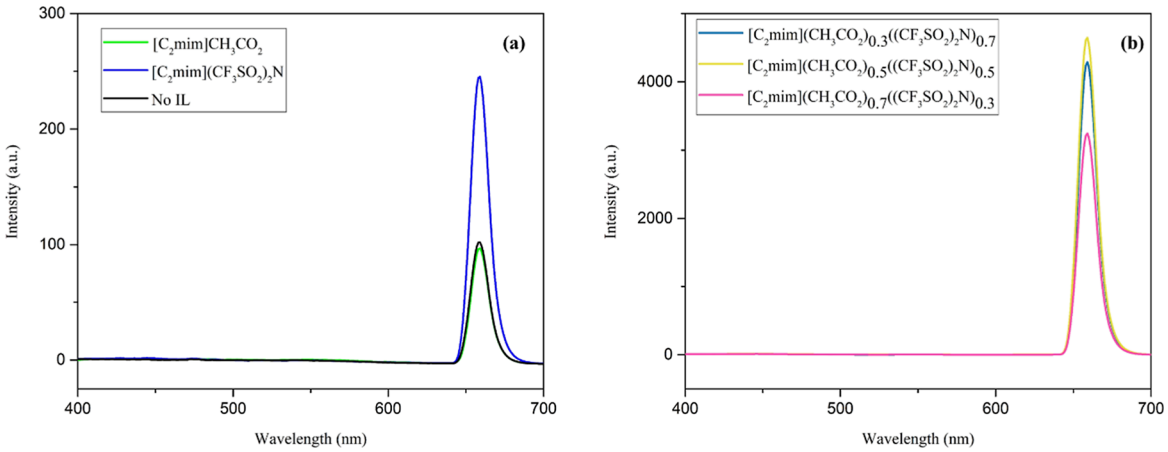

Figure 5. Room-temperature PL spectra (defect emission) of ZnO NPs obtained from (a) pure ILs and without ILs and (b) DSILs.

as well as the front/back facets of the disks, so that in this medium the disks experienced an incomplete growth; hence, the interpenetrated structure was observed.

Thus, $[C_2mim](CH_3CO_2)_{0.7}((CF_3SO_2)_2N)_{0.3}$ was effective to produce interpenetrated hexagonal disks which could not be obtained from any of the two pure ILs. This is one of the advantages of the DSILs over pure ILs. Another important factor is the uniformity of the particles obtained from $[C_2mim](CH_3CO_2)_{0.5}((CF_3SO_2)_2N)_{0.5}$, which was not observed in the case of pure ILs such as $[C_2mim](CF_3SO_2)_2N$. A delicate balance of the two anions in $[C_2mim](CH_3CO_2)_{0.5}((CF_3SO_2)_2N)_{0.5}$ was accountable for the formation of uniform-sized particles rather than the pure IL and other two DSILs. In the case of $[C_2mim](CH_3CO_2)_{0.5}((CF_3SO_2)_2N)_{0.5}$, both of the anions collectively enhanced their roles in the formation of NPs with uniform size. These two anions cooperatively decreased their limitations when acting separately in these certain aspects for the synthesis of ZnO NPs. The synergistic effect observed in DSILs helped to overcome the restrictions of the pure ILs, and it also revealed the means to achieving fascinating shapes of the NPs which could not be realized from the individual ILs.

The HRTEM images in Figure 4 further support the hypotheses made from the XRD and FESEM analyses. The structure of the NPs obtained without any IL was found to be cylindrical prism-shaped (Figure 4a). The interplanar spacing (*d*-spacing) of the lattice stripes was found to be 0.26 nm which corresponds to the distance between two adjacent (002) planes. This suggests the preferred growth of ZnO NPs along the [0001] crystal axis. The SAED pattern shows individual bright spots which are almost in a circular pattern. This reveals that without any IL, ZnO forms larger grains that create the prism-shaped particles which are polycrystalline in nature. Because of the bigger grains which are mainly single crystals, there are bright individual spots in the SAED pattern. With the introduction of $[C_2mim]CH_3CO_2$ in the reaction medium, the structure of the ZnO NPs transformed into disk-shaped which can be observed in Figure 4b. The average length of the hexagonal crystallites is 23 nm. The *d*-spacing is found to be 0.25 nm, corresponding to the (101) plane, which suggests the preferred growth axis to be the [1010] axis. This is also confirmed from the previous discussion that $[C_2mim]CH_3CO_2$ drives the growth along the [1010] direction by protecting the (001) planes of the hexagon. The SAED pattern confirms the polycrystalline nature of the obtained nanostructures. On the contrary, Figure 4c represents the *d*-spacing to be 0.29 nm, which corresponds to the (100) plane. This suggests that the preferred growth direction of the ZnO NPs obtained from the $[C_2mim](CF_3SO_2)_2N$ medium is the [0001] crystal axis. Moreover, the nanodice-shaped particle is observed along with the tendency to form nanorod-shaped structure. The SAED pattern proves the polycrystalline nature; however, there are bright spots in the pattern that suggest the bigger single crystals or grains that forms the nanodice.

Figure 4d represents the HRTEM image of the ZnO nanostructure obtained from the DSIL, $[C_2mim](CH_3CO_2)_{0.3}((CF_3SO_2)_2N)_{0.7}$. The darkest spots indicate that the hexagonal disks have been agglomerated due to the cumulative effect of the anions. This is also supported by the FESEM images where the hexagonal disks were closing toward each other, forming an agglomeration of disks. The SAED pattern reveals the polycrystalline nature of the unique nanostructures. $[C_2mim](CH_3CO_2)_{0.5}((CF_3SO_2)_2N)_{0.5}$ provides the incomplete hexagonal disk shape that has been initiated to become interpenetrated (Figure 4e). The darker spots clearly represent the closeness of the disks. Also, the incomplete growth is caused by the combined effect of the two anions present in the DSIL. Consequently, the SAED pattern proves the polycrystalline nature of the NPs. Finally, at the highest molar ratio of the $CH_3CO_2^-$ anion, the obtained ZnO NPs form the interpenetrated hexagonal disk structure to exhibit dark spots in Figure 4f as the evidence of the interpenetration of the hexagonal disks. Moreover, the SAED pattern shows the polycrystallinity of the NPs, but the pattern has only bright spots and no circular rings. This indicates that larger hexagonal single crystals got closer and then interpenetrated into each other by the synergistic effect of both the anions present in $[C_2mim](CH_3CO_2)_{0.7}((CF_3SO_2)_2N)_{0.3}$. For the three DSILs, the *d*-spacing observed was 0.25 nm, and in each case, the main structure of the particle was hexagonal disk. The $CH_3CO_2^-$ anion played the dominant role of controlling the shape of the nanostructures rather than the $(CF_3SO_2)_2N^-$ anion.

The HRTEM images further prove the role of pure ILs and DSILs to control the growth of ZnO NPs and act as a superior soft template. The introduction of ILs/DSILs not only decreased the size of the particles but also preferred a unique growth direction for the controlled growth of the clusters to achieve exquisite architectures of the NPs. Nevertheless, DSILs

https://doi.org/10.1021/acsomega.3c09374
ACS Omega 2024, 9, 12992−13005

provided a better control over their parent ILs in controlling the size and shape of the nanostructures.

The analysis of E_g of the nanostructures indicates the greater influence of size toward the optical properties of ZnO NPs. Since ZnO is an n-type semiconductor, E_g is crucial for its applications. The E_g value of the NPs from different media has been measured via the DRS technique with the help of the Kubelka−Munk method (Figure S3 and Table S6). The smallest band gap (2.94 eV) was found for the particles obtained when no IL was used. With the addition of ILs, enhanced E_g was observed. Moreover, the DSILs provided the highest E_g (3.27 eV), indicating crystalline particles with smaller size. According to the quantum confinement effect, the particle size variation with the E_g value could be explained. The size quantization (Q-size) effect manifests when the confinement of charge carriers causes the size of the semiconductor particle to decrease from its bulk to that of the Bohr radius, for example, in the first excitation state. As a result, electrons and holes are contained in a potential well in the quantum-sized semiconductor and do not experience the delocalization that occurs in the bulk phase. Because of this, the band gap widens as the size of an ultrafine semiconductor particle approaches the band gap minimum. The variation of band gap energy is related to the size of the NPs, and this variation is consistent with the size distribution observed by DLS measurements.

The fascinating phenomenon of enhancement of semiconductor property depending on the shape and size of the NPs would be useful in the field of optoelectronic device technology. Consequently, the photoluminescence (PL) spectral analysis of the product NPs has been performed for the investigation of the optoelectronic property of the ZnO NPs. The fluorescence spectra for all the prepared NPs were taken at the excitation wavelength of 325 nm. Figure 5 shows the PL spectra of ZnO NPs obtained from pure ILs and DSILs.

The UV emission had an extremely low intensity compared to the defect emission intensity. An intense sharp peak was present for all of the samples at the wavelength of 658 nm which corresponds to red emission. According to the findings of Lima et al., the red emission is caused by one of the intrinsic defects, singly charged oxygen vacancy (V_o^+).[54] It may also be responsible for the neutral Zn interstitial (Zn_i).[55] Neutral oxygen vacancy could also cause the strong defect emission peak.[54,55] Either one could be responsible for the defect observed, or even combined intrinsic defects could also be vital in this case.[55] For identifying the defect present in the synthesized ZnO, a simple representation of defect energy states (responsible for red emission) found in ZnO is given in the schematic diagram in Figure S4. The probability of the neutral oxygen vacancies would be the best option to cause the emission that was followed by the NPs synthesized in this work. These defects should be on the surface of ZnO NPs. With one oxygen vacancy per 64 oxygen atoms, the static dielectric constant is increased by 1−2% for neutral vacancies.[56] Thus, the defect could be used for the advancement of electrical properties of semiconductor-based devices. Also, the absorption phenomena of the NPs could be significantly influenced by the presence of oxygen vacancies. This suggests the potential of these NPs for various optical applications.

Another important factor is the intensity of the peak (Figure 5), which is different for each of the ZnO NPs obtained from different ILs or DSILs. Figure 5a shows that ZnO NPs obtained from $[C_2mim](CF_3SO_2)_2N$ have stronger intensity, while ZnO prepared in the absence of any IL and $[C_2mim]CH_3CO_2$ gives a lower intensity. The intensity of emission can be correlated with the increasing electronic defects located into the forbidden band. The fluorescence strength is proportional to the number of vacancies and/or defects, so the larger the axial dimension, the stronger the emission is.[53] Thus, the NPs of the shape of mostly dice-like particles obtained from $[C_2mim](CF_3SO_2)_2N$ provided a higher intensity than those of smaller disk- or prism-shaped NPs acquired with $[C_2mim]CH_3CO_2$ and without any IL, respectively. Similarly, the variation of intensity in Figure 5b could be explained. In this case, ZnO NPs from $[C_2mim](CH_3CO_2)_{0.5}((CF_3SO_2)_2N)_{0.5}$ provided the highest intensity, and $[C_2mim](CH_3CO_2)_{0.3}((CF_3SO_2)_2N)_{0.7}$ gave the second highest peak and $[C_2mim](CH_3CO_2)_{0.7}((CF_3SO_2)_2N)_{0.3}$ the third highest one. All these intensities are way higher than the intensities observed in Figure 5a. As seen in FESEM images, the aggregation behavior of NPs obtained from DSILs could be understood. This caused the enlarged axial dimensions of the particles, and the most aggregated disks were explored in the case of $[C_2mim](CH_3CO_2)_{0.5}((CF_3SO_2)_2N)_{0.5}$ to provide the highest intensity. In the case of $[C_2mim](CH_3CO_2)_{0.7}((CF_3SO_2)_2N)_{0.3}$, as the disks were interpenetrated, reducing the axial dimensions, it showed a lesser intensity. Consequently, the third highest peak observed for $[C_2mim](CH_3CO_2)_{0.3}((CF_3SO_2)_2N)_{0.7}$ could be explained as it provided only disk-like particles with less assembly. However, this disk was found with greater axial dimensions than all the other shapes observed from the pure ILs. Therefore, the emission intensity could be explained for all the ZnO NPs.

Attempts have been made to elucidate the mechanism of formation of ZnO nanostructures. The NPs were produced from two ILs and three different DSILs. The introduction of DSILs into the synthesis of ZnO nanostructures gave the scope to optimize the composition to unveil the ZnO−IL interaction. It also paved the way of investigating the pros and cons of using DSILs over pure IL regarding the production of uniform-size NPs with a specific shape. First of all, creation of $Zn(OH)_2$, which produces the equivalent $Zn(OH)_4^{2-}$ complex when hydroxide ions are present, is considered to be the pathway via which ZnO is formed. ZnO is produced when these latter species undergo dehydration upon heating. Reactions involved in the formation of ZnO are displayed in Scheme 1.

Scheme 1. Reactions Involved in the Formation of ZnO

$$Zn(NO_3)_2.6H_2O + 2NaOH \longrightarrow Zn(OH)_2 + 2Na^+ + 2NO_3^- + 6H_2O \quad (1)$$

$$Zn(OH)_2 + 2OH^- \longrightarrow Zn(OH)_4^{2-} \quad (2)$$

$$Zn(OH)_4^{2-} \xrightarrow{\triangle} ZnO \quad (3)$$

The variations of shapes of ZnO NPs prepared from the ILs and DSILs took place because of the specific growth direction managed by the IL media and the protection of certain facets of the NP provided by the ILs/DSILs. The self-assembled structure of the ILs/DSILs was possible due to the hydrogen-bonding system or $\pi-\pi$ stacking mechanism. Because of its ability to extract electrons from the bulk through the sharing of an electron pair between hydrogen and carbon at position 2 of the imidazole ring,[53] the imidazolium cation of the ILs used in this work should interact with the bulk via a hydrogen bond or

https://doi.org/10.1021/acsomega.3c09374
ACS Omega 2024, 9, 12992−13005

Scheme 2. Schematic Illustration of (A) Formation Process of the ZnO Nanostructures and (B) Effect of Concentration of ILs and DSILs

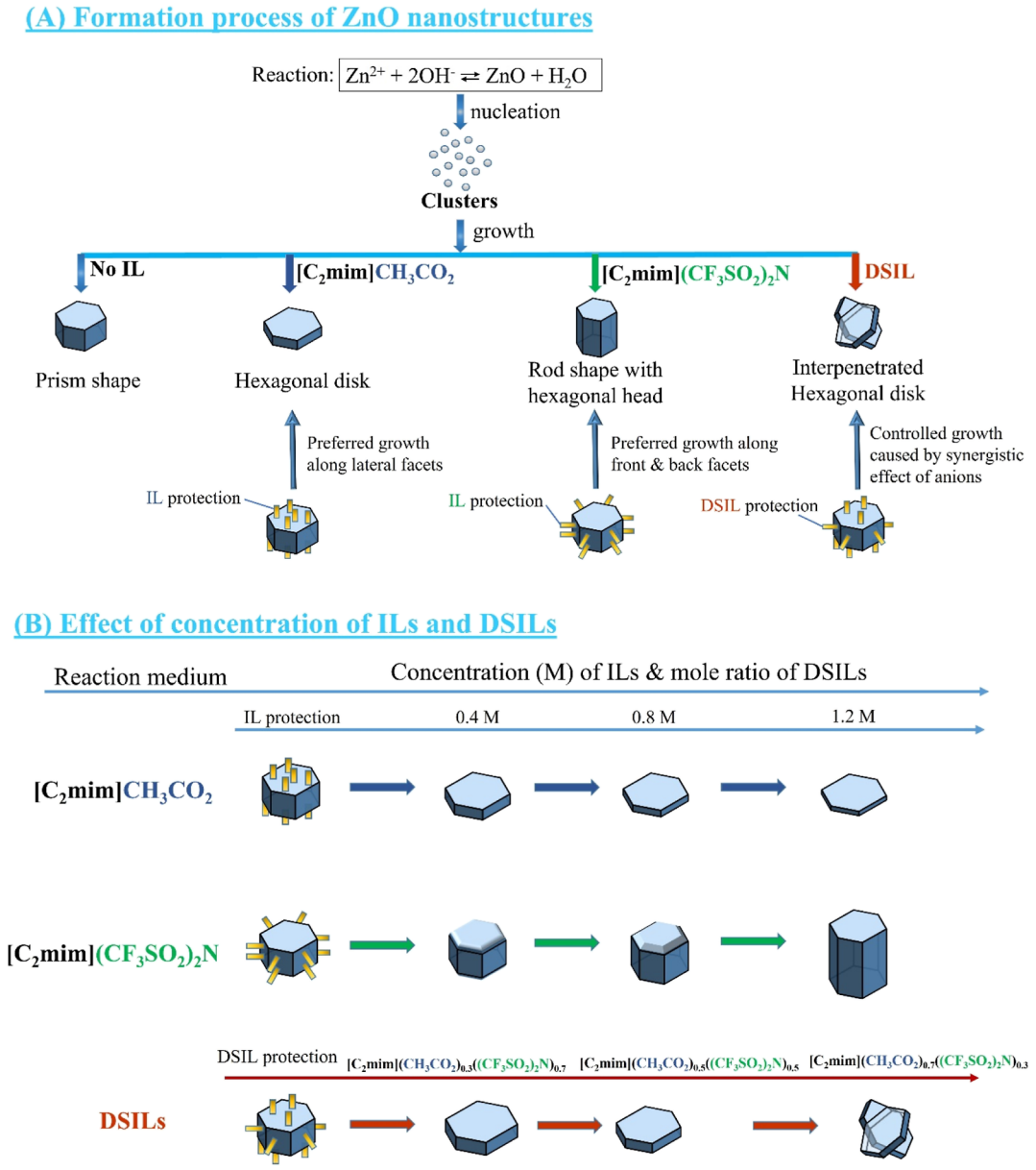

electrostatic force. These interactions accumulate and stack, potentially through $\pi-\pi$ stacking or other noncovalent interactions between the generated nanostructures and imidazolium rings. Consequently, the IL is adsorbed on the surface of the developing ZnO crystals, enclosing a portion of the forming material and causing the crystal to grow in an anisotropic manner. This means that it is possible for the ZnO material to be encouraged by the ILs to form ZnO nanostructures through a hydrogen-bonding co-stack mechanism.[57,58] Since all the ILs/DSILs used in this work have the same cation, it can be concluded that both the $\pi-\pi$ stacking and hydrogen bonding would have the same effect on controlling the morphology.[59,60] However, the different anions would affect these interactions between the cation and product ZnO NPs and ultimately control the packing of the soft template around the growing NPs.[61] Now, it is necessary to know which growth direction was promoted by the ILs/DSILs in this work and which portion of the growing ZnO was protected by them to avoid further growth. $[C_2mim]CH_3CO_2$ provided disk-like nanostructures due to the presence of the $CH_3CO_2^-$ anion, which promoted the growth along the [1010] direction and protected the front and back facets of the hexagonal disk. With the increasing concentration of this anion, the protection seemed to get stronger as the thickness of the disk followed a decreasing trend with the higher concentration of the IL. On the contrary, $[C_2mim](CF_3SO_2)_2N$ provided dice- or rod-like particles due to the promoted growth at the [0001] direction and the protection of the lateral facets by the presence of $(CF_3SO_2)_2N^-$ anion. Also, with the increasing concentration of $(CF_3SO_2)_2N^-$ anion, the protection of the lateral facets was grown to produce rods with lower width than dices. However, when both of the anions were present in the case of DSILs, there was a combined effect of the anions which was liable for the interpenetrated disk-like shape. However, the $CH_3CO_2^-$ anion showed dominance over the $(CF_3SO_2)_2N^-$ anion as the thickness of the disks decreased

https://doi.org/10.1021/acsomega.3c09374
ACS Omega 2024, 9, 12992−13005

Scheme 3. Schematic Representation of Interaction Between a ZnO Crystal and (a) $[C_2mim]CH_3CO_2$, (b) $[C_2mim](CF_3SO_2)_2N$, and (c) DSIL

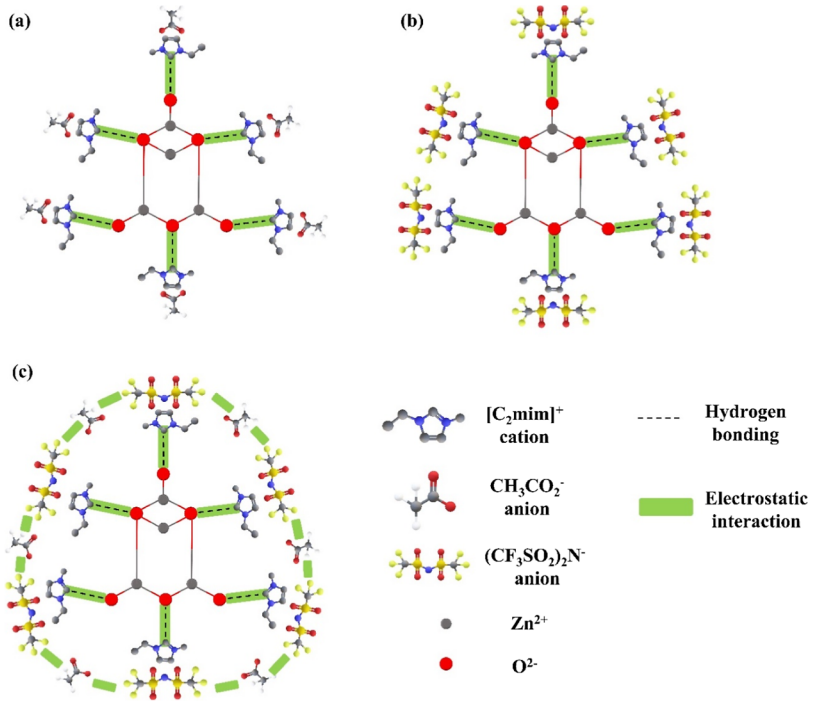

with the higher content of $CH_3CO_2^-$ in the DSIL. The presence of $CH_3CO_2^-$ anion protected the front and back facets, while the protection of the lateral facets by the $(CF_3SO_2)_2N^-$ anion caused the disks to be pushed closer and closer which ended up with an incomplete growth and interpenetration of the disks. This overall ZnO−IL interaction is represented in Scheme 2.

Scheme 2A refers to the selective adsorption phenomenon of different ILs on the surface of the growing ZnO. The anions of the two pure ILs individually controlled the growth direction in a different manner. Since the geometry of all the NPs was the same, it could have been influenced by the common cation and $CH_3CO_2^-$ anion dominantly. However, the DSILs provided the cooperative influence of the two anions so that the interpenetrated disk shape was observed. In this case, the lateral facets of the hexagonal disks which were preferably protected by the $(CF_3SO_2)_2N^-$ anion were less protected or rather pushed by the $(CF_3SO_2)_2N^-$ anion due to the presence of the $CH_3CO_2^-$ anion. Thus, while the front and back facets were protected by the $CH_3CO_2^-$ anion, the presence of $(CF_3SO_2)_2N^-$ anion caused the disks to come closer and at a point the disks came into each other. This is how these two anions synergistically acted to provide the interpenetrated disk shape.

Scheme 2B provides the simplest representation of the concentration effect of the ILs. The change in concentration significantly affected the shape and size of the ZnO NPs. At the higher concentrations of $[C_2mim][CH_3CO_2]$, the disk thickness reduced, while for $[C_2mim](CF_3SO_2)_2N$, the dice-shaped prism gradually decreased in width to produce rod-shaped particles at higher concentrations. Thus, interpenetration occurred in the case of DSILs where each of the two anions performed their individual role to produce the collective effect. The cation and two anions collectively formed a specific growth direction where the growth rate was controlled significantly in order to produce sharper crystals.

Scheme 3 represents the interaction of the ZnO crystal with ILs and DSILs. The self-assembled structure of the ILs/DSILs through the hydrogen-bonding system or $\pi-\pi$ stacking mechanism is displayed here. The anions of pure ILs can direct the growth specifically, but in the case of DSIL, the presence of both anions caused extra electrostatic interactions between the anions to bring about a change in the surrounding atmosphere of the ZnO crystal. This greatly influenced the nucleation rate to be higher than the growth rate, and thus the smallest crystallite size was observed from the DSIL. Also, this could be responsible for the incomplete growth or interpenetration of the hexagonal disk shape. Being smaller in size, the $CH_3CO_2^-$ anion retained its compacting behavior, while the $(CF_3SO_2)_2N^-$ anion pushed them away from the adsorbed cation. Therefore, the anions almost surrounded the growing crystal, which resulted in the special size and shape of the ZnO nanostructure.

4. CONCLUSIONS

ZnO NPs could be successfully synthesized from pure ILs and DSILs using a hydrothermal route. ILs act as a soft template where the DSILs provided an exceptionally better performance. Both the pure ILs, $[C_2mim]CH_3CO_2$ and $[C_2mim]$-$(CF_3SO_2)_2N$, provided particles of smaller size at the concentration of 0.8 M. DSILs provided particles of less than 100 nm in size, which corresponds to the cooperative effects observed from the anions in the DSIL media. However, in all cases, uniformity of particle size was noticed when the concentration of pure ILs increased, and for DSILs, uniformity was achieved at the same mole ratio of the anions. Highly crystalline products of wurtzite structure were confirmed from all the reaction media among which the DSIL produced the smallest crystallite size. The morphology of the synthesized

https://doi.org/10.1021/acsomega.3c09374
ACS Omega 2024, 9, 12992−13005

NPs was transformed into hexagonal disks from prism shape with the addition of $[C_2mim]CH_3CO_2$ whose growing concentration caused the production of perfect hexagon geometry with sharper edges. However, $[C_2mim](CF_3SO_2)_2N$ provided dice-like nanostructures which ultimately formed a rodlike shape with hexagonal heads at the highest concentration of the IL. Moreover, incomplete or interpenetrated hexagonal disks were obtained from $[C_2mim]$-$(CH_3CO_2)_{0.7}((CF_3SO_2)_2N)_{0.3}$, proving that the individual effects of $CH_3CO_2^-$ and $(CF_3SO_2)_2N^-$ anions synergistically affected the shape in the case of DSILs. Strong red emission and negligible UV emission were observed for ZnO NPs to demonstrate their potential for optoelectronic devices. This study suggests that DSILs can be a better choice than their component pure ILs to get specific control over the shape of the NPs. Also, the nucleation rate and the growth of ZnO clusters could be managed by DSILs via the collective effect of the two anions. This mechanism of formation of ZnO NPs and the fundamental observations from this work would be significant for the development of future research on the synthesis of ZnO NPs from DSILs of this kind.

■ ASSOCIATED CONTENT

Supporting Information

The Supporting Information is available free of charge at https://pubs.acs.org/doi/10.1021/acsomega.3c09374.

Characterization of the produced NPs (FTIR and EDX analysis), detailed analysis of XRD data (crystallite size and relative intensity ratio calculation), morphological investigation from FESEM images (detailed geometry analysis of the hexagons), and band gap energy analysis and photoluminescence spectral analysis of the product NPs (PDF)

■ AUTHOR INFORMATION

Corresponding Author

Md. Abu Bin Hasan Susan − *Department of Chemistry, University of Dhaka, Dhaka 1000, Bangladesh; Dhaka University Nanotechnology Centre (DUNC), University of Dhaka, Dhaka 1000, Bangladesh;* orcid.org/0000-0003-0752-1979; Phone: +8809666911463 ext. 7162; Email: susan@du.ac.bd; Fax: +88 0255167810

Authors

Md. Arif Faisal − *Department of Chemistry, University of Dhaka, Dhaka 1000, Bangladesh*

Saika Ahmed − *Department of Chemistry, University of Dhaka, Dhaka 1000, Bangladesh*

Complete contact information is available at: https://pubs.acs.org/10.1021/acsomega.3c09374

Notes

The authors declare no competing financial interest.

■ ACKNOWLEDGMENTS

The authors acknowledge Dhaka University to provide Article Publishing Charges under the International Publication Grant of Dhaka University. The Research Grant of DU-UGC is gratefully acknowledged. M.A.F. also acknowledges Semiconductor Technology Research Centre of the University of Dhaka, Bangladesh, for a research fellowship. The authors express their gratitude to the Centre for Advanced Research in Sciences of Dhaka University, Bangladesh, for permitting the use of XRD and photoluminescence spectrophotometer. The authors also acknowledge analytical services from the Genome Centre of Jashore University of Science and Technology, Bangladesh, for FESEM and EDX and the Sophisticated Test and Instrumentation Centre, India, for HRTEM and SAED.

■ REFERENCES

(1) Tavakoli, A.; Sohrabi, M.; Kargari, A. A Review of Methods for Synthesis of Nanostructured Metals with Emphasis on Iron Compounds. *Chem. Pap.* **2007**, *61*, 151−170.

(2) Liu, W. T. Nanoparticles and Their Biological and Environmental Applications. *J. Biosci. Bioeng.* **2006**, *102* (1), 1−7.

(3) Ju-Nam, Y.; Lead, J. R. Manufactured Nanoparticles: An Overview of Their Chemistry, Interactions and Potential Environmental Implications. *Sci. Total Environ.* **2008**, *400* (1−3), 396−414.

(4) Caruso, F.; Caruso, R. A.; Möhwald, H. Nanoengineering of Inorganic and Hybrid Hollow Spheres by Colloidal Templating. *Science* **1998**, *282* (5391), 1111−1114.

(5) Sun, Y.; Xia, Y. Shape-Controlled Synthesis of Gold and Silver Nanoparticles. *Science* **2002**, *298* (5601), 2176−2179.

(6) Mondal, C.; Pal, J.; Ganguly, M.; Sinha, A. K.; Jana, J.; Pal, T. A One Pot Synthesis of Au-ZnO Nanocomposites for Plasmon-Enhanced Sunlight Driven Photocatalytic Activity. *New J. Chem.* **2014**, *38* (7), 2999−3005.

(7) Maiti, S.; Pal, S.; Chattopadhyay, K. K. Recent Advances in Low Temperature, Solution Processed Morphology Tailored ZnO Nanoarchitectures for Electron Emission and Photocatalysis Applications. *CrystEngComm* **2015**, *17* (48), 9264−9295.

(8) Kowsari, E.; Bazri, B. Synthesis of Rose-like ZnO Hierarchical Nanostructures in the Presence of Ionic Liquid/Mg^{2+} for Air Purification and Their Shape-Dependent Photodegradation of SO_2, NO_x, and CO. *Appl. Catal., A* **2014**, *475*, 325−334.

(9) Hancock, J. M.; Rankin, W. M.; Hammad, T. M.; Salem, J. S.; Chesnel, K.; Harrison, R. G. Optical and Magnetic Properties of ZnO Nanoparticles Doped with Co, Ni and Mn and Synthesized at Low Temperature. *J. Nanosci. Nanotechnol.* **2015**, *15* (5), 3809−3815.

(10) Beek, W. J. E.; Wienk, M. M.; Janssen, R. A. J. Efficient Hybrid Solar Cells from Zinc Oxide Nanoparticles and a Conjugated Polymer. *Adv. Mater.* **2004**, *16* (12), 1009−1013.

(11) Shohel, M.; Miran, M. S.; Susan, M. A. B. H.; Mollah, M. Y. A. Calcination Temperature-Dependent Morphology of Photocatalytic ZnO Nanoparticles Prepared by an Electrochemical-Thermal Method. *Res. Chem. Intermed.* **2016**, *42* (6), 5281−5297.

(12) Thomas, D. G. The Exciton Spectrum of Zinc Oxide. *J. Phys. Chem. Solids* **1960**, *15* (1−2), 86−96.

(13) Dvorak, M.; Wei, S. H.; Wu, Z. Origin of the Variation of Exciton Binding Energy in Semiconductors. *Phys. Rev. Lett.* **2013**, *110* (1), 016402.

(14) Su, Y. Q.; Zhu, Y.; Yong, D.; Chen, M.; Su, L.; Chen, A.; Wu, Y.; Pan, B.; Tang, Z. Enhanced Exciton Binding Energy of ZnO by Long-Distance Perturbation of Doped Be Atoms. *J. Phys. Chem. Lett.* **2016**, *7* (8), 1484−1489.

(15) Garcia, M. A.; Merino, J. M.; Fernández Pinel, E.; Quesada, A.; De La Venta, J.; Ruíz González, M. L.; Castro, G. R.; Crespo, P.; Llopis, J.; González-Calbet, J. M.; Hernando, A. Magnetic Properties of ZnO Nanoparticles. *Nano Lett.* **2007**, *7* (6), 1489−1494.

(16) Xu, H.; Zhao, Q.; Yang, H.; Chen, Y. Study of Magnetic Properties of ZnO Nanoparticles Codoped with Co and Cu. *J. Nanopart. Res.* **2009**, *11* (3), 615−621.

(17) Sirelkhatim, A.; Mahmud, S.; Seeni, A.; Kaus, N. H. M.; Ann, L. C.; Bakhori, S. K. M.; Hasan, H.; Mohamad, D. Review on Zinc Oxide Nanoparticles: Antibacterial Activity and Toxicity Mechanism. *Nano-Micro Lett.* **2015**, *7* (3), 219−242.

(18) Xie, Y.; He, Y.; Irwin, P. L.; Jin, T.; Shi, X. Antibacterial Activity and Mechanism of Action of Zinc Oxide Nanoparticles against Campylobacter Jejuni. *Appl. Environ. Microbiol.* **2011**, *77* (7), 2325−2331.

(19) Emami-Karvani, Z.; Chehrazi, P. Antibacterial Activity of ZnO Nanoparticle on Gram-Positive and Gram-Negative Bacteria. *Afr. J. Microbiol. Res.* **2011**, *5* (12), 1368−1373.
(20) Duan, X.; Huang, Y.; Agarwal, R.; Lieber, C. M. Single-Nanowire Electrically Driven Lasers. *Nature* **2003**, *421* (6920), 241−245.
(21) Barrelet, C. J.; Greytak, A. B.; Lieber, C. M. Nanowire Photonic Circuit Elements. *Nano Lett.* **2004**, *4* (10), 1981−1985.
(22) Law, M.; Sirbuly, D. J.; Johnson, J. C.; Goldberger, J.; Saykally, R. J.; Yang, P. Nanoribbon Waveguides for Subwavelength Photonics Integration. *Science* **2004**, *305* (5688), 1269−1273.
(23) Wang, Z. L. Zinc Oxide Nanostructures: Growth, Properties and Applications. *J. Phys.: Condens. Matter* **2004**, *16* (25), R829−R858.
(24) Wang, X.; Ding, Y.; Summers, C. J.; Wang, Z. L. Large-Scale Synthesis of Six-Nanometer-Wide ZnO Nanobelts. *J. Phys. Chem. B* **2004**, *108* (26), 8773−8777.
(25) Moharram, A. H.; Mansour, S. A.; Hussein, M. A.; Rashad, M. Direct Precipitation and Characterization of ZnO Nanoparticles. *J. Nanomater.* **2014**, *2014*, 1−5.
(26) Antonietti, M.; Kuang, D.; Smarsly, B.; Zhou, Y. Ionic Liquids for the Convenient Synthesis of Functional Nanoparticles and Other Inorganic Nanostructures. *Angew. Chem., Int. Ed.* **2004**, *43*, 4988−4992.
(27) Zhou, Y.; Schattka, J. H.; Antonietti, M. Room-temperature ionic liquids as template to monolithic mesoporous silica with wormlike pores via a sol- gel nanocasting technique. *Nano Lett.* **2004**, *4* (3), 477−481.
(28) Lian, J.; Duan, X.; Ma, J.; Peng, P.; Kim, T.; Zheng, W. Hematite (α-Fe_2O_3) with various morphologies: ionic liquid-assisted synthesis, formation mechanism, and properties. *ACS Nano* **2009**, *3* (11), 3749−3761.
(29) Lian, J.; Kim, T.; Liu, X.; Ma, J.; Zheng, W. Ionothermal synthesis of turbostratic boron nitride nanoflakes at low temperature. *J. Phys. Chem. C* **2009**, *113* (21), 9135−9140.
(30) Noda, A.; Susan, M. A. B. H.; Kudo, K.; Mitsushima, S.; Hayamizu, K.; Watanabe, M. Brønsted Acid−Base Ionic Liquids as Proton-Conducting Nonaqueous Electrolytes. *J. Phys. Chem. B* **2003**, *107* (17), 4024−4033.
(31) Susan, M. A. B. H.; Kaneko, T.; Noda, A.; Watanabe, M. Ion Gels Prepared by in Situ Radical Polymerization of Vinyl Monomers in an Ionic Liquid and Their Characterization as Polymer Electrolytes. *J. Am. Chem. Soc.* **2005**, *127* (13), 4976−4983.
(32) Papageorgiou, N.; Athanassov, Y.; Armand, M.; Bonhôte, P.; Pettersson, H.; Azam, A.; Grätzel, M. The Performance and Stability of Ambient Temperature Molten Salts for Solar Cell Applications. *J. Electrochem. Soc.* **1996**, *143* (10), 3099−3108.
(33) Tokuda, H.; Hayamizu, K.; Ishii, K.; Susan, M. A. B. H.; Watanabe, M. Physicochemical Properties and Structures of Room Temperature Ionic Liquids. 1. Variation of Anionic Species. *J. Phys. Chem. B* **2004**, *108* (42), 16593−16600.
(34) Susan, M. A. B. H.; Noda, A.; Mitsushima, S.; Watanabe, M. Brønsted acid−base ionic liquids and their use as new materials for anhydrous proton conductors. *Chem. Commun.* **2003**, No. 8, 938−939.
(35) Susan, M. A. B. H.; Saha, S.; Ahmed, S.; Begum, F.; Rahman, M. M.; Mollah, M. Y. A. Electrodeposition of Cobalt from a Hydrophilic Ionic Liquid at Ambient Condition. *Mater. Res. Innovations* **2012**, *16* (5), 345−349.
(36) Wittmar, A.; Gautam, D.; Schilling, C.; Dörfler, U.; Mayer-Zaika, W.; Winterer, M.; Ulbricht, M. Stable Zinc Oxide Nanoparticle Dispersions in Ionic Liquids. *J. Nanopart. Res.* **2014**, *16* (5), 2341.
(37) Rabieh, S.; Bagheri, M. Effect of Ionic Liquid [C_4mim]Cl on Morphology of Nanosized-Zinc Oxide. *Mater. Lett.* **2014**, *122*, 190−192.
(38) Husanu, E.; Cappello, V.; Pomelli, C. S.; David, J.; Gemmi, M.; Chiappe, C. Chiral Ionic Liquid Assisted Synthesis of Some Metal Oxides. *RSC Adv.* **2017**, *7* (2), 1154−1160.
(39) Zhang, M.; Xu, X.; Zhang, M. Hydrothermal Synthesis of Sheaf-like CuO via Ionic Liquids. *Mater. Lett.* **2008**, *62* (3), 385−388.
(40) Chatel, G.; Pereira, J. F. B.; Debbeti, V.; Wang, H.; Rogers, R. D. Mixing Ionic Liquids-"simple Mixtures" or "Double Salts"? *Green Chem.* **2014**, *16*, 2051−2083.
(41) Peck, R. L.; Brink, N. G.; Kuehl, F. A.; Flynn, E. H.; Walti, A.; Folkers, K. Streptomyces Antibiotics. II. Crystalline Streptomycin Trihydrochloride-Calcium Chloride Double Salt. *J. Am. Chem. Soc.* **1945**, *67*, 1866−1867.
(42) Miran, M. S.; Yasuda, T.; Susan, M. A. B. H.; Dokko, K.; Watanabe, M. Binary Protic Ionic Liquid Mixtures as a Proton Conductor: High Fuel Cell Reaction Activity and Facile Proton Transport. *J. Phys. Chem. C* **2014**, *118* (48), 27631−27639.
(43) Pereiro, A. B.; Araújo, J. M. M.; Oliveira, F. S.; Bernardes, C. E. S.; Esperança, J. M. S. S.; Canongia Lopes, J. N.; Marrucho, I. M.; Rebelo, L. P. N. Inorganic Salts in Purely Ionic Liquid Media: The Development of High Ionicity Ionic Liquids (HIILs). *Chem. Commun.* **2012**, *48* (30), 3656−3658.
(44) Annat, G.; Forsyth, M.; MacFarlane, D. R. Ionic Liquid Mixtures-Variations in Physical Properties and Their Origins in Molecular Structure. *J. Phys. Chem. B* **2012**, *116* (28), 8251−8258.
(45) Kunze, M.; Jeong, S.; Paillard, E.; Winter, M.; Passerini, S. Melting Behavior of Pyrrolidinium-Based Ionic Liquids and Their Binary Mixtures. *J. Phys. Chem. C* **2010**, *114* (28), 12364−12369.
(46) Finotello, A.; Bara, J. E.; Narayan, S.; Camper, D.; Noble, R. D. Ideal Gas Solubilities and Solubility Selectivities in a Binary Mixture of Room-Temperature Ionic Liquids. *J. Phys. Chem. B* **2008**, *112* (8), 2335−2339.
(47) Tominaga, K. ichi. An Environmentally Friendly Hydroformylation Using Carbon Dioxide as a Reactant Catalyzed by Immobilized Ru-Complex in Ionic Liquids. *Catal. Today* **2006**, *115* (1−4), 70−72.
(48) Lee, S. H.; Ha, S. H.; Hiep, N. M.; Chang, W. J.; Koo, Y. M. Lipase-Catalyzed Synthesis of Glucose Fatty Acid Ester Using Ionic Liquids Mixtures. *J. Biotechnol.* **2008**, *133* (4), 486−489.
(49) Richard, A. R.; Adidharma, H. The Performance of Ionic Liquids and Their Mixtures in Inhibiting Methane Hydrate Formation. *Chem. Eng. Sci.* **2013**, *87*, 270−276.
(50) Zhao, Q.; Anderson, J. L. Highly Selective GC Stationary Phases Consisting of Binary Mixtures of Polymeric Ionic Liquids. *J. Sep. Sci.* **2010**, *33* (1), 79−87.
(51) Akai, N.; Kawai, A.; Shibuya, K. First Observation of the Matrix-isolated FTIR Spectrum of Vaporized Ionic Liquid: An Example of EmimTFSI, 1-Ethyl-3-methylimidazolium Bis-(trifluoromethanesulfonyl)imide. *Chem. Lett.* **2008**, *37* (3), 256−257.
(52) Andeen, D.; Kim, J. H.; Lange, F. F.; Goh, G. K. L.; Tripathy, S. Lateral Epitaxial Overgrowth of ZnO in Water at 90 °C. *Adv. Funct. Mater.* **2006**, *16* (6), 799−804.
(53) Qi, K.; Yang, J.; Fu, J.; Wang, G.; Zhu, L.; Liu, G.; Zheng, W. Morphology-Controllable ZnO Rings: Ionic Liquid-Assisted Hydrothermal Synthesis, Growth Mechanism and Photoluminescence Properties. *CrystEngComm* **2013**, *15* (34), 6729−6735.
(54) Lima, S. A. M.; Sigoli, F. A.; Jafelicci Jr, M.; Davolos, M. R. Luminescent Properties and Lattice Defects Correlation on Zinc Oxide. *Int. J. Inorg. Mater.* **2001**, *3* (7), 749−754.
(55) Lin, B.; Fu, Z.; Jia, Y. Green Luminescent Center in Undoped Zinc Oxide Films Deposited on Silicon Substrates. *Appl. Phys. Lett.* **2001**, *79* (7), 943−945.
(56) Cockayne, E. Influence of Oxygen Vacancies on the Dielectric Properties of Hafnia: First-Principles Calculations. *Phys. Rev. B: Condens. Matter Mater. Phys.* **2007**, *75* (9), 094103.
(57) Rajiv Gandhi, R.; Gowri, S.; Suresh, J.; Sundrarajan, M. Ionic Liquids Assisted Synthesis of ZnO Nanostructures: Controlled Size, Morphology and Antibacterial Properties. *J. Mater. Sci. Technol.* **2013**, *29* (6), 533−538.
(58) Akter, M.; Satter, S. S.; Singh, A. K.; Rahman, M. M.; Mollah, M. Y. A.; Susan, M. A. B. H. Hydrophilic Ionic Liquid-Assisted Control of the Size and Morphology of ZnO Nanoparticles Prepared

https://doi.org/10.1021/acsomega.3c09374
ACS Omega 2024, 9, 12992−13005

by a Chemical Precipitation Method. *RSC Adv.* **2016**, *6* (94), 92040−92047.
(59) Sharma, R. K.; Chouryal, Y. N.; Chaudhari, S.; Saravanakumar, J.; Dey, S. R.; Ghosh, P. Adsorption-driven Catalytic and Photocatalytic Activity of Phase Tuned In_2S_3 Nanocrystals Synthesized via Ionic Liquids. *ACS Appl. Mater. Interfaces* **2017**, *9* (13), 11651−11661.
(60) Ghosh, P.; Mudring, A. V. Phase Slective Synthesis of Quantum Cutting Nanophosphors and the Observation of a Spontaneous Room Temperature Phase Transition. *Nanoscale* **2016**, *8* (15), 8160−8169.
(61) Akter, M.; Faisal, M. A.; Singh, A. K.; Susan, M. A. B. H. Hydrophilic Ionic Liquid Assisted Hydrothermal Synthesis of ZnO Nanostructures with Controllable Morphology. *RSC Adv.* **2023**, *13* (26), 17775−17786.

https://doi.org/10.1021/acsomega.3c09374
ACS Omega 2024, 9, 12992−13005